

Multi-objective and multi-case reliability-based design optimization for tailor rolled blank (TRB) structures

Guangyong Sun^{1,2} · Huile Zhang¹ · Jianguang Fang² · Guangyao Li¹ · Qing Li²

Received: 14 April 2016 / Revised: 10 September 2016 / Accepted: 14 September 2016 / Published online: 17 October 2016
© Springer-Verlag Berlin Heidelberg 2016

Abstract Light weight and crashworthiness signify two main challenges facing in vehicle industry, which often conflict with each other. In order to achieve light weight while improving crashworthiness, tailor rolled blank (TRB) has become one of the most potential lightweight technologies. To maximize the characteristics of TRB structures, structural optimization has been adopted extensively. Conventional optimization studies have mainly focused on a single loading case (SLC). In practice, however, engineering structures are often subjected to multiple loading cases (MLC), implying that the optimal design under a certain condition may no longer be an optimum under other loading cases. Furthermore, traditional deterministic optimization could become less meaningful or even unacceptable when uncertainties of design variables and noises of system parameters are present. To address these issues, a multi-objective and multi-case reliability-based design optimization (MOMCRBDO) was developed in this study to optimize the TRB hat-shaped structure. The radial basis function (RBF) metamodel was adopted to approximate the responses of objectives and constraints, the non-dominated sorting genetic algorithm II (NSGA-II), coupled with Monte Carlo Simulation (MCS), was employed to seek optimal reliability solutions. The optimal results show that the proposed method is not only capable of improving the reliability of Pareto solutions, but also enhancing the robustness under MLC.

Keywords Reliability based design optimization · Crashworthiness · Tailor rolled blank · Multiple loading cases · Multi-objective optimization

1 Introduction

The research attention in automotive industry has been paid to vehicle lightweight and crashworthiness due to ever-growing requirements in environmental concerns, government legislations and consumer demanding (Sun et al. 2010). Unfortunately, these two performances always conflict with each other. To maintain crashworthiness performance during vehicular lightweighting, high strength steel (HSS) and ultra-high strength steel (UHSS) have been widely adopted to replace conventional steel. In this regard, the Ultralight Steel Auto Body (ULSAB) project achieved a body-in-white (BIW) weight reduction of 68 kg (from 271 kg to 203 kg) by using HSS (Kim et al. 2010). Zhang et al. (2006) developed a rule to carry out lightweight design of automobile parts by replacing mild steel with HSS, which was validated by numerical simulations. Jiang et al. (2012) designed the door beam with UHSS to realize full marks of crash tests, with a stiffness increase of 2.5 times, strength increase of 3.8 times, and weight reduction of 9.32%.

Although the aforementioned methods of material substitution can reduce vehicle weight effectively, the high prices of these materials hinder their large-scale application in a highly competitive market. Moreover, conventional uniform thickness structures may not exert their maximum capacities of crashworthiness and light weight. Therefore, tailor welded blank (TWB) process has been developed as an advanced manufacturing technology. TWB structures are manufactured by welding metal sheets with different materials and/or thickness prior to the forming process (Merklein et al. 2014). Thus,

✉ Guangyao Li
gyli@hnu.edu.cn

¹ State Key Laboratory of Advanced Design and Manufacture for Vehicle Body, Hunan University, Changsha 410082, China

² School of Aerospace, Mechanical and Mechatronic Engineering, The University of Sydney, Sydney, NSW 2006, Australia

not only does it save materials appreciably, but also provides a more flexible combination of different sheets. In this regard, frontal side rails, the inner door panels and B-pillars are some typical examples (Li et al. 2015; Pan et al. 2010; Shi et al. 2007; Xu et al. 2013). However, since the material properties in the thermal influence zone can be rather different from base materials, potentially causing stress concentration and leading to high risk of fatigue failure. The transverse movement of seam during deep drawing is disadvantageous and the seam could abrade the tools significantly (Hirt et al. 2005).

Recently, a new rolling technology, namely tailor rolled blank (TRB), is developed to overcome these defects of TWB. Compared with TWB, TRBs allow a continuous transition between the thick and thin zones leading to better formability and a higher surface quality. Furthermore, the production cost of TRBs is independent of the number of thickness transitions (Merklein et al. 2014). To understand the crushing behaviors of TRB, TRB thin-walled structures under axial and lateral impacts have been studied recently (Sun et al. 2015b; Sun et al. 2014). For example, Sun et al. (2014) investigated the crashworthiness of a square TRB tube under an axial impact. Chuang et al. (2008) adopted the TRB manufacturing technology for designing a vehicle underbody. Duan et al. (2016) redesigned a front longitudinal beam using the TRB technology, and claimed that the weight of FLB was reduced by 15.21%, whereas the crashworthiness was improved compared with the baseline design.

While there have been some studies on the design of TRB structures, most of them were conducted under a specific loading case. As a matter of fact, practical engineering structures are often subjected to multiple load cases (MLC), implying that an optimal design under a certain loading condition may not meet the performance requirements under other loading conditions (Fang et al. 2015a). The literature indicated that although structural optimization allows enhancing crashworthiness of vehicle in a specific loading case, the effectiveness of optimization could be challenged if different crushing velocities and directions are considered (Duddeck and Wehrle 2015; Zhang et al. 2014). From a design perspective, an optimum is expected to accommodate not only a single loading case (SLC), but also MLC. In this regard, Zhang et al. (2014) proposed a dual weight factor method to optimize the hollow and conical tubes under MLC. Qiu et al. (2015) investigated the multi-cell hexagonal tube under MLC by using complex proportional assessment and multi-objective optimization approaches.

Furthermore, these abovementioned MLC designs were largely restricted to deterministic optimization, in which all design parameters involved are certain. However, engineering problems inevitably involve uncertainties in loads, geometry, material properties and operational conditions, etc., in which a deterministic optimization could lead to unreliable or unstable designs thereby increasing risk of design failure (Choi et al. 2006; Fang et al. 2014; Yang and Gu 2004; Fang et al. 2016). Therefore,

many nondeterministic optimization algorithms have been proposed to take into account the effects of various uncertainties (Cheng et al. 2006; Youn and Choi 2004) and effectively resolved design problems in real-life (Du and Chen 2004; Fang et al. 2015b; Gu et al. 2013b; Li et al. 2011; Zhu et al. 2011). In this regard, Du and Chen (2004) proposed the sequential optimization and reliability assessment (SORA) method and used in reliability-based design for vehicle crashworthiness of side impact. Chen et al. (2013) developed an optimal shifting vector approach to enhancing the efficiency of reliability-based design optimization (RBDO) for the design of honeycomb cellular structures. Fang et al. (2013) presented a reliability-based multi-objective design optimization for the design of a vehicle door. To the authors' best knowledge, however, there have been limited studies on the multi-objective reliability-based design optimization (MORBDO) for multiple loading case problems.

The rest of the paper is organized as follows: Section 2 proposes the mathematical modeling of multi-objective and multi-case reliability-based design optimization (MOMCRBDO) procedure and relevant algorithms, including Monte Carlo simulation (MCS), radial basis function (RBF) metamodeling and the non-dominated sorting genetic algorithm II (NSGA-II) optimization. In Section 3, the finite element modeling of TRB hat-shaped (TRBHS) structures are developed and then the quasi-static axial crushing and drop-hammer impact tests are performed to validate the accuracy of the FE models. Section 4 depicts the optimization process of MOMCRBDO for TRBHS, followed by the results and discussions. Finally, Section 5 draws some conclusions.

2 Methods for design analysis and optimization

2.1 Multi-objective and multi-case reliability-based design optimization

Generally speaking, engineering structures likely have to be operated in MLC, and thus a design is expected to be an optimum under MLC. A multi-objective deterministic design optimization (MODDO) under MLC can be formulated as follows (Qiu et al. 2015):

$$\left\{ \begin{array}{l} \min \quad \sum_{k=1}^q \lambda_k f_{i,k}(\mathbf{x}) \quad i = 1, 2, \dots, m \\ \text{s.t.} \quad g_{j,k}(\mathbf{x}) \leq 0 \quad j = 1, 2, \dots, n \\ \quad \quad \sum_{k=1}^q \lambda_k = 1 \quad \lambda_k \geq 0 \\ \quad \quad \mathbf{x}^L \leq \mathbf{x} \leq \mathbf{x}^U \end{array} \right. \quad (1)$$

where \mathbf{x} denotes the vector of design variables, $f_{i,k}(\mathbf{x})$ is the i th objective under the k th load case; $g_{j,k}(\mathbf{x})$ is the j th inequality

constraint function; m and n are the numbers of objective functions and inequality constraints, respectively; λ_k is the weighting factor to reflect the relative importance and/or occurrence probability of the k th loading case, q represents the number of load cases considered; \mathbf{x}^L and \mathbf{x}^U are the lower and upper bounds, respectively. Eq. (1) is a typical deterministic optimization problem.

To obtain the multi-objective reliable optimization under MLC, MOMCRBDO is explored in this study. Different from the deterministic optimization, reliability-based design seeks an optimum subject to certain probabilistic constraints, mathematically expressed as:

$$\left\{ \begin{array}{l} \min \quad \sum_{k=1}^q \lambda_k f_{i,k}(\mathbf{x}) \quad i = 1, 2, \dots, m \\ \text{s.t.} \quad p[g_{j,k}(\mathbf{x}) \leq 0] \geq R_{j,k} \quad j = 1, 2, \dots, n \\ \quad \quad \sum_{k=1}^q \lambda_k = 1 \quad \lambda_k \geq 0 \\ \quad \quad \mathbf{x}^L \leq \mathbf{x} \leq \mathbf{x}^U \end{array} \right. \quad (2)$$

where the design feasibility is formulated as the probability ($p[\cdot]$) of constraint satisfaction (i.e., $g_{j,k}(\mathbf{x}) \leq 0$) bigger than or equal to a desired probability $R_{j,k}$.

2.2 Monte Carlo simulation (MCS) method

The MOMCRBDO problems in Eq. (2) always involve a procedure to evaluate the failure probability or reliability of constraints. Many reliability analysis methods have been developed, including the approximation methods (e.g., the first order and second order reliability analysis methods), direct integration, and sampling methods (e.g., MCS). Among which, MCS is the most commonly used approach for its accuracy and applicability (Gu and Yang 2005).

Mathematically, the failure probability p_f can be formulated by the multivariate integration, given as (Melchers 1987):

$$p_f = \int_{g(\mathbf{x}) \leq 0} f(\mathbf{x}) d\mathbf{x} = \int_{-\infty}^{+\infty} I[g(\mathbf{x}) \leq 0] f(\mathbf{x}) d\mathbf{x} = E\{I[g(\mathbf{x}) \leq 0]\} \quad (3)$$

where \mathbf{x} is the vector of random parameters, $g(\mathbf{x})$ is the performance function defined such that failure occurs when $g(\mathbf{x}) < 0$, $f(\mathbf{x})$ is the joint probability density function, $I[\cdot]$ is the indicator function for event $g(\mathbf{x}) < 0$, having the value 1 if event $g(\mathbf{x}) < 0$ and value 0 otherwise. $E\{\cdot\}$ is the expectation of the indicator function.

According to Eq. (3), p_f can be evaluated using MCS as follows:

$$\hat{p}_f = \frac{1}{N} \sum_{i=1}^N I_{[g(\mathbf{x}_i) \leq 0]}(\mathbf{x}_i) \quad (4)$$

where \hat{p}_f is the estimated failure probability, and N is the number of sample points, \mathbf{x}_i for $i = 1, 2, \dots, N$ are the sample points generated according to $f(\mathbf{x})$.

The accuracy of MCS estimation can be quantified with the standard error, defined as:

$$\text{error} = \frac{\sigma_f(\mathbf{x})}{\sqrt{N}} \quad (5)$$

The error is therefore unrelated to the problem dimension (i.e., the number of design variables), which is very appealing for large-scale problems. And the error is proportional to $1/\sqrt{N}$, implying that the improvement of accuracy by one order of magnitude will require 100 times more samples. Such computational cost can be prohibitive in application for complex and highly nonlinear problems.

On the other hand, the minimum sampling size required for the failure probability level $p[g(\mathbf{x}) \leq 0]$ as suggested by (Tu et al. 1999) is:

$$L = \frac{10}{p[g(\mathbf{x}) \leq 0]} \quad (6)$$

which indicates that for a 10% estimated probability of failure; about 100 function evaluations (e.g., FEA runs) are required with some confidence on the first digit of failure prediction. To verify an event having a 1% failure probability; about 1000 structural analyses are required, which would be usually considered too expensive for some engineering applications. To improve computational efficiency, MCS combined with metamodels, has been employed to quantify the failure probability, which makes a great number of model evaluations feasible (Abdessalem and El-Hami 2015; Fang et al. 2013; Jansson et al. 2008).

2.3 Metamodeling

Crashworthiness optimization requires a considerable number of nonlinear finite element (FE) runs which typically leads to high computational cost, especially for a MOMCRBDO problem in Eq. (2). As an alternative, the metamodeling techniques have been widely used, which can largely reduce the number of FE runs. In this regard, the radial basis function (RBF) has exhibited a fairly good accuracy for highly nonlinear problems (Fang et al. 2005; Sun et al. 2011; Xu et al. 2013) and was utilized to construct the metamodel for responses in this study.

To construct a metamodel accurately, design of experiment (DOE) needs to be first employed to sample the design space. Among many available DOE approaches, the optimal Latin hypercube sampling (OLHS) (Park

1994; Sun et al. 2012) has proven effective and was implemented here to generate sample points. Then, the responses of these sample points need to be evaluated by FEA for constructing RBF models.

A typical RBF model can be formulated as (Hardy 1971):

$$f(x) = \sum_{i=1}^N w_i \phi(\|\mathbf{x}-\mathbf{x}_i\|) + \sum_{j=1}^M c_j p_j(\mathbf{x}) \quad (7)$$

where N is the number of sampling points, $\|\mathbf{x}-\mathbf{x}_i\|$ is the Euclidean norm of design variable vectors \mathbf{x} and the i th sampling point \mathbf{x}_i , ϕ is a basis function, w_i is the unknown weighting factor positioned at the i th sampling point; M is the number of polynomial terms, $p_j(\mathbf{x})$ are the polynomial terms and c_j is the corresponding coefficient for $p_j(\mathbf{x})$, usually $M < N$. Obviously, an RBF model is actually a linear combination of N radial basis functions and M polynomial terms with the weighted coefficients.

Of those feasible basis functions, the multi-quadric formulation (specifically $\phi(r) = \sqrt{r^2 + c^2}$, where c is the free shape parameter) was chosen for its prediction accuracy as well as commonly linear and possibly exponential rate of convergence with increasing sampling points (Acar et al. 2011). More discussion about RBF in crashworthiness design can be found in literature (Fang et al. 2005).

It should be noted that RBF passes through all sample points, meaning that the fitness accuracy of an approximate function from the existing sampling points cannot be checked directly. For this reason, a series of additional validation points were generated to verify the accuracy of the constructed metamodelling. Three different fitting indicators, namely R -square (R^2), relative average absolute error (RAAE) and relative maximum absolute error (RMAE), are employed here (Jin et al. 2001) and given as

$$R^2 = 1 - \frac{\sum_{i=1}^K (y_i - \hat{y}_i)^2}{\sum_{i=1}^K (y_i - \bar{y})^2} \quad (8)$$

$$RAAE = \frac{\sum_{i=1}^K |y_i - \hat{y}_i|}{\sum_{i=1}^K |y_i - \bar{y}_i|} \quad (9)$$

$$RMAE = \frac{\max\{|y_1 - \hat{y}_1|, \dots, |y_K - \hat{y}_K|\}}{\sum_{i=1}^K |y_i - \hat{y}_i| / K} \quad (10)$$

where K is the number of newly generated validation points, y_i is the true values, \hat{y}_i is the corresponding approximate metamodel value, and \bar{y} is the mean of y_i . In general, the larger the R^2 values, the more accurate the metamodel. The smaller the RAAE and RMAE, the better the metamodel.

2.4 Non-dominated sorting genetic algorithm II (NSGA-II)

In this study, the NSGA-II (Deb et al. 2002) was employed to obtain the non-dominated optimal solutions for the multi-objective optimization problem. The main features of NSGA lie in that it ranks solutions with non-dominated sorting and assigns them in fitness based on their ranks. While the crossover and mutation operators remain similar to a simple GA, the selection operator distinguishes itself. As an improvement of NSGA, NSGA-II is characterized by a fast non-dominated sorting procedure that is an elitist strategy, a parameter-less diversity-preservation mechanism and a simple yet efficient constraint-handling method. Many crashworthiness design problems (Gu et al. 2013a; Gu et al. 2013b; Liao et al. 2008; Xu et al. 2013) have been successfully solved using NSGA-II. The details of NSGA-II can be found in Deb et al. (2002).

During the optimization progress, accurate RBF models were first constructed with the given weighting factors for different loading case. Then, the NSGA-II algorithm was employed to perform the deterministic and non-deterministic optimization with MCS. For clarification, the proposed MOMCRBDO procedure for the crashworthiness optimization of TRB structures is further depicted in the flowchart (Fig. 1).

3 Numerical modeling and experimental validation

3.1 Description of geometrical features

The front longitudinal beam is the most significant energy-absorbing component for frontal impacts, and its collapse modes and energy absorbing capability can greatly influence the full vehicle crashworthiness and safety of passengers. To simplify the complexity of real front longitudinal beam, a representative TRB hat-shaped (TRBHS) structure was extracted for design analysis and optimization, as shown in Fig. 2.

The TRBHS specimen consists of a hat-shaped sheet and a bottom sheet which are joined by spot-welding along the center line of the flange with a spot diameter of 5mm at an interval of 30 mm, as shown in Fig. 3a.

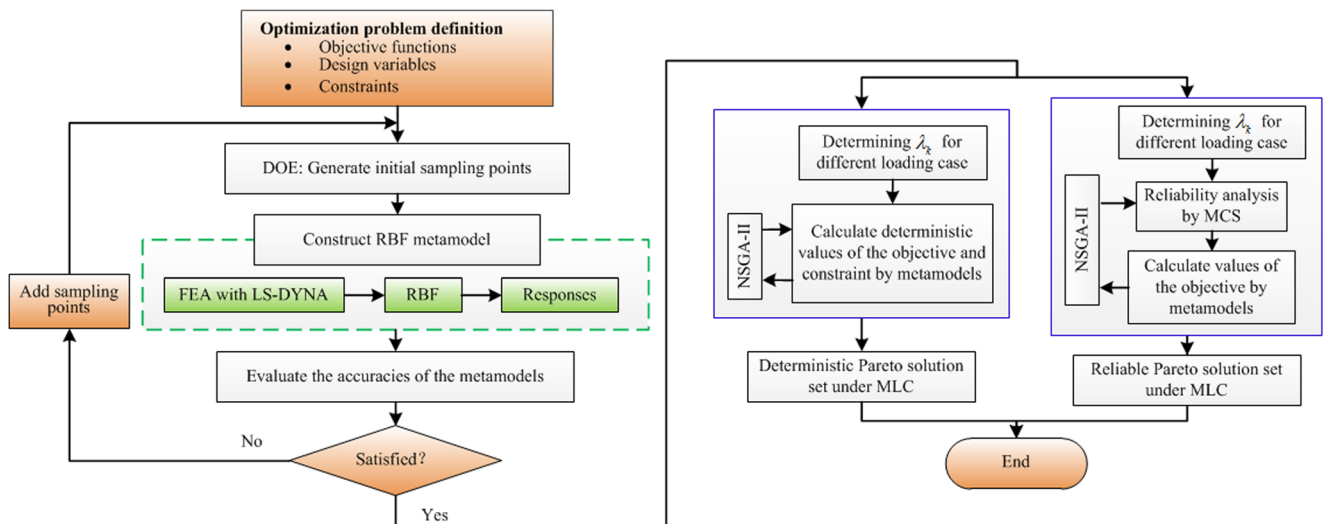


Fig. 1 The flowchart of multi-objective and multi-case reliability-based design optimization

These two sheets are divided into three different thickness zones, namely thin zone, thick zone and thickness transition zone (TTZ), respectively. The total length and the flange width of TRBHS are $L=400$ mm and 30 mm, respectively. The corner radii near the weld flange and at the top edges are $R=4$ mm. The other detailed dimensions of the TRBHS are illustrated in Table 1. The transition slope of the TTZ are set as 1:100 to meet the economic requirement (Hirt et al. 2005). Herein, the length of the TTZ, l_2 in Fig. 3b, is 40 mm.

3.2 Numerical modeling

3.2.1 Material constitutive model for TRB

To systematically understand the crashworthiness characteristics of TRBHS, the finite element models under



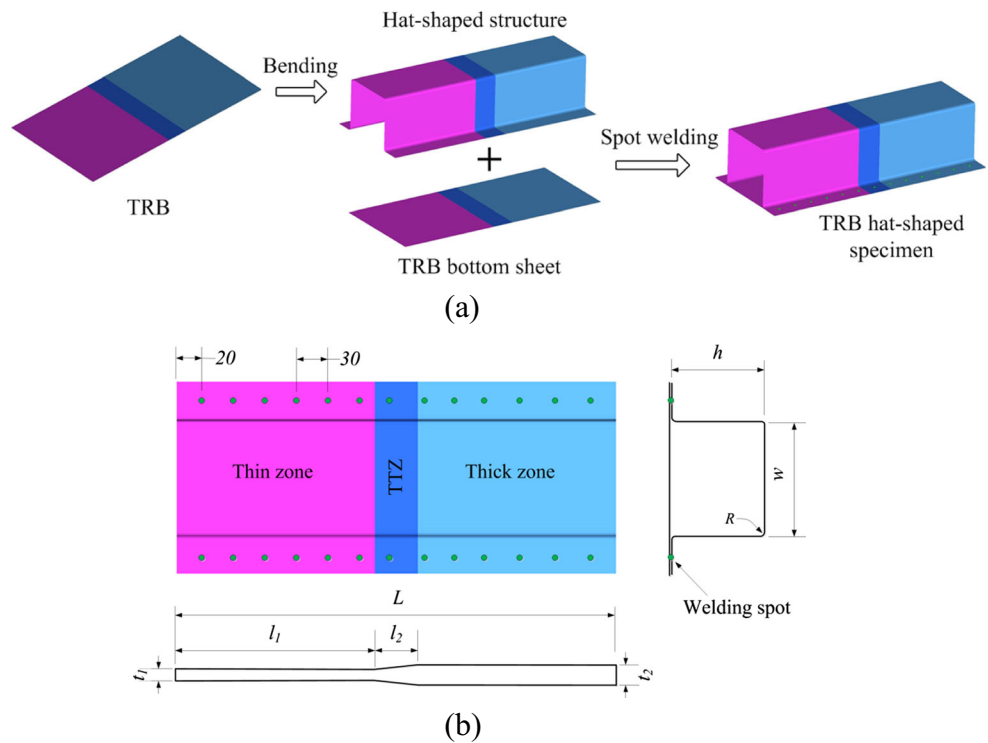
Fig. 2 The typical hat-shaped structure in vehicle

quasi-static loading case and dynamic loading case were established. The material of hat-shaped specimen considered herein is high-strength steel HSLA 340, whose density, Poisson's ratio and Young's modulus are 7.8×10^3 kg/m³, 0.3 and 210 GPa, respectively. To consider the non-uniform material properties of TRB due to the variable thickness, Duan et al. (2016) have developed the effective stress vs. effective strain relation of TRBs made of HSLA 340 by the Lagrange polynomial interpolation, as illustrated in Fig. 4. Based on the interpolation surface in Fig. 4b, the material properties can be obtained for any thickness.

3.2.2 Finite element modeling

The explicit nonlinear FE code LS-DYNA was employed to simulate the crashworthiness of the TRBHS. Figure 5 shows the FE model of the TRBHS subjected to axial impact. The 4-node quadrilateral Belytschko-Lin-Tsay shell elements with reduced integration were used to model the TRBHS walls. To model the thickness variation more realistically, different thicknesses were assigned to four nodes of the shell elements using the keyword *ELEMNET_SHELL_THICKNESS in LS-DYNA (Hallquist 2007), as shown in Fig. 6. Five integration points were employed across the thickness to capture the local element bending, and stiffness-type hourglass control was utilized to eliminate spurious zero energy models. The constitutive behavior of HSLA340 was modeled via the piecewise linear plasticity material model, MAT 24, in LS-DYNA (Hallquist 2007; Kopp et al. 2005). To accurately consider the different material properties in the different thicknesses, the elements with nearly the same thickness were

Fig. 3 Description of **a** manufacturing process, **b** the dimensions of the TRBHS



defined as one component and each component was assigned its own mechanical properties that were interpolated from the effective stress vs. effective strain relationship (i.e. Fig. 4) as illustrated in Fig. 6. To determine the proper mesh size, several simulations were carried out and an element size of 3×3 mm was found sufficient for the numerical simulations. The two parts of the TRBHS were welded together along the center line of the flange by employing a constrained spot-weld option.

The FE model of quasi-static axial crushing tests is shown in Fig. 5a, where the two platens were both modeled to be rigid and the bottom one was fixed. A constant velocity $V=5$ mm/min was applied to the top platen to gradually crush the specimen. The contact between the specimen and two rigid walls was modeled using “automatic node to surface” algorithm. The “automatic single surface” algorithm was employed to the specimen itself to avoid interpenetration during axial collapse.

Figure 5b shows the FE modeling of dynamic impact tests. The bottom of the specimen was fixed to a rigid wall and a

rigid platen impacted onto the specimen at an initial velocity of 8 m/s with an additional mass of 706 kg. The “automatic single surface” algorithm was defined to simulate the self-contact of the specimen in buckling and “automatic node to surface” algorithm was defined between the specimen and the two rigid walls. The static and dynamic coefficients of frictions were set as 0.35 and 0.25, respectively.

Since HSLA340 is a strain-rate sensitive material, the strain-rate effect should be taken into account. In this study, the effect was accounted for using the Cowper-Symonds model given as (Hallquist 2007):

$$\sigma_y(\epsilon_{eff}^p, \epsilon_{eff}^p) = \sigma_y^s(\epsilon_{eff}^p) \left[1 + \left(\frac{p}{C} \right)^{1/p} \right] \tag{11}$$

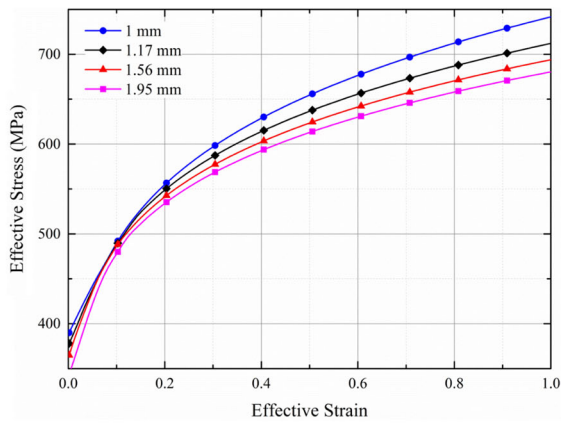
where $\sigma_y(\epsilon_{eff}^p, \epsilon_{eff}^p)$ is the dynamic yield stress, $\sigma_y^s(\epsilon_{eff}^p)$ is the static stress and ϵ_{eff}^p is the strain rate. C and p denote two strain-rate parameters.

3.3 Experimental validation

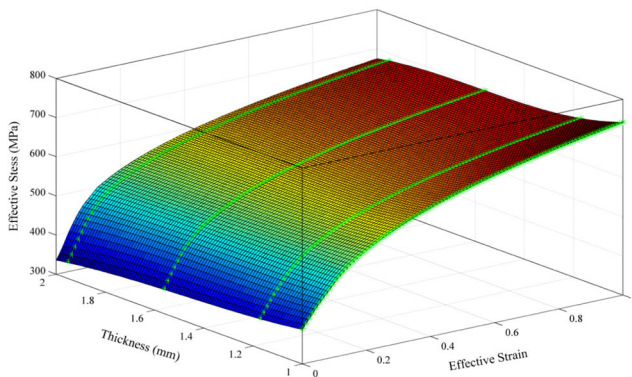
To validate the TRBHS modeling accuracy under different loading cases, the quasi-static crushing test and the drop-hammer impact test were carried out in this study.

Table 1 The dimensions of the TRBHS

Parameters	t_1	t_2	l_1	w	h
Dimension (mm)	1.2	1.6	180	105	85



(a)



(b)

Fig. 4 Effective stress–strain relationship **a** Different thicknesses, **b** Interpolation surface (Duan et al. 2016)

3.3.1 Experimental details

The quasi-static crushing tests were performed in a standard universal testing machine MTS647, as shown in Fig. 7. To ensure a central crushing, two steel plates

were respectively placed at the upper and lower end of the specimens without other constraints. The thin zone of the TRBHS specimens was placed at the incident (top) end for all the tests to generate progressive folding collapses. A constant crushing speed of 5 mm/min was set. The total compression displacement was set as a constant of 270 mm, which represents 67.5% of the specimen length.

The drop-hammer impact tests were performed in a dynamic test rig, as illustrated in Fig. 8. To prevent the toppling of the specimens, a steel plate was welded to the bottom end of the specimens. The other steel plate was placed at the top end of the specimens to ensure a central loading. The dynamic procedure was conducted at the initial impact velocity 8 m/s with an additional mass of 706 kg.

3.3.2 Validation of the FE model

To systematically study the crashworthiness of structures, crashworthiness indicators, i.e., peak crash fore (F_{max}) and energy absorption (EA), were usually used, as shown in Fig. 5c.

The EA of a structure subjected to the axial compression loading can be calculated as:

$$EA = \int_0^{d_{max}} F(x)dx \tag{12}$$

where d_{max} is the maximum crushing distance, $F(x)$ denotes crushing force. The peak value of $F(x)$ during the whole crushing progress is denoted as F_{max} .

The experimental and corresponding simulation results are given in Figs. 9 and 10, respectively. It is clear that the force versus displacement and energy versus

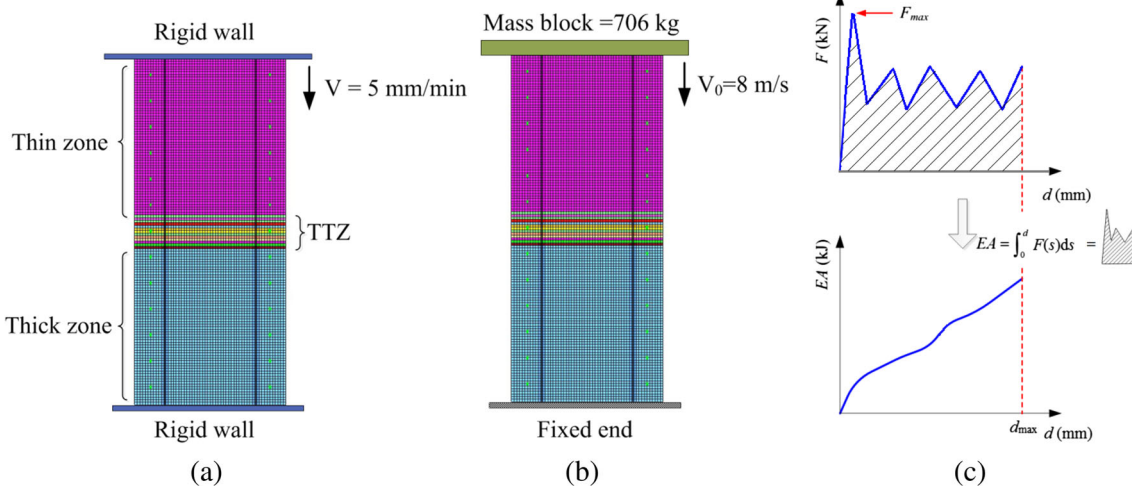


Fig. 5 Schematic of **a** quasi-static axial crushing tests **b** dynamic impact tests **c** indicators of axial crushing

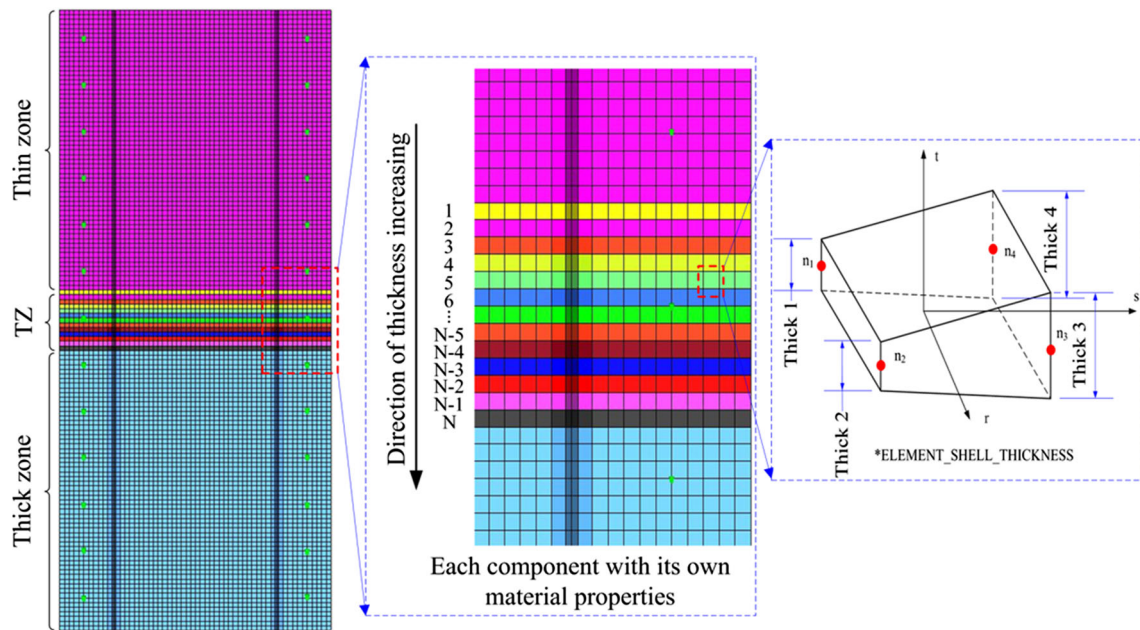


Fig. 6 Schematic of FE modeling of TRB with a variable thickness

displacement curves of the FE simulation agree well with the experimental results. Moreover, the deformation modes of the simulation match very well with those of the experiments. The satisfactory correlations suggested that the FE models is able to well predict the crash process of the TRBHS specimen and can be employed for the further design analysis and optimization.

3.3.3 Numerical results and discussion

To better understand the crashworthiness of TRBHS under axial crushing loading, a range of TRBHSs with different dimensions were investigated using the FE simulation. As shown in Table 2, Case 0 is the experimentally-validated model. Other cases were modeled to investigate the effects of the thicknesses of the thin and thick zones (t_1, t_2), the position of TTZ (l_1) and sectional dimensions (w, h) of TRBHS on crashworthiness. For Cases 1 to 4, only one

parameter was changed each time to quantify the parametric influence by comparing with Case 0. All the cases in this study were summarized in Table 2.

Figures 11 and 12 plot the histograms of crashworthiness indicators (i.e., F_{max} and EA), respectively. From these two figures, it is easily found that the structural parameters significantly affect the TRBHS crashworthiness. Specifically, F_{max} is strongly influenced by the thickness of thin zone (t_1) while EA is affected by all the structural parameters considered. Note that greater values of the thicknesses of the thin and thick zones (t_1, t_2) can improve EA , but a larger value of the thickness of the thin zone (t_1) influences F_{max} negatively. Besides, EA decreased with the increase in the length of thin zone (l_1) and the effect of sectional dimensions on EA is far greater than that on F_{max} . More importantly, the change trends of design variables to the crashworthiness indicators significantly differ under the quasi-static and dynamic crashes, further reinforcing the strategy of design optimization under MLC.

Fig. 7 Quasi-static axial crushing tests setup

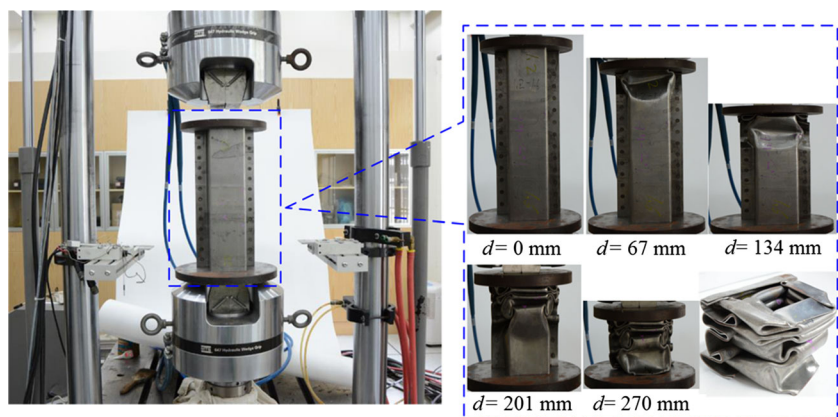
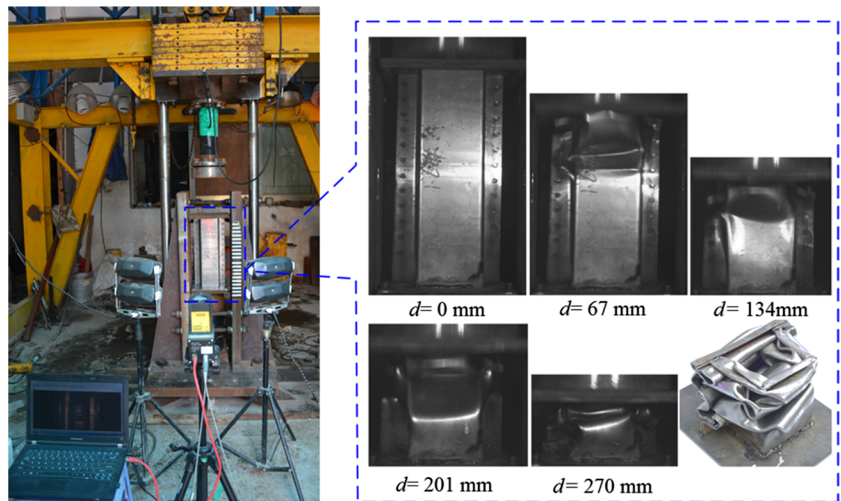


Fig. 8 Drop-hammer impact test setup



4 Multi-objective and multi-case reliability-based design optimization

4.1 Definition of optimization problem

For addressing crashworthiness and lightweight criteria, the design optimization presented here aims to maximize energy

absorption and minimize the mass, while limiting the peak force during collapse (White and Jones 1999). Thus, the EA and mass M of TRBHS are chosen as objective functions, whilst the peak force F_{max} should be constrained within a certain level. To account for the effects of different loading cases, the deterministic multi-objective optimization problem can be defined

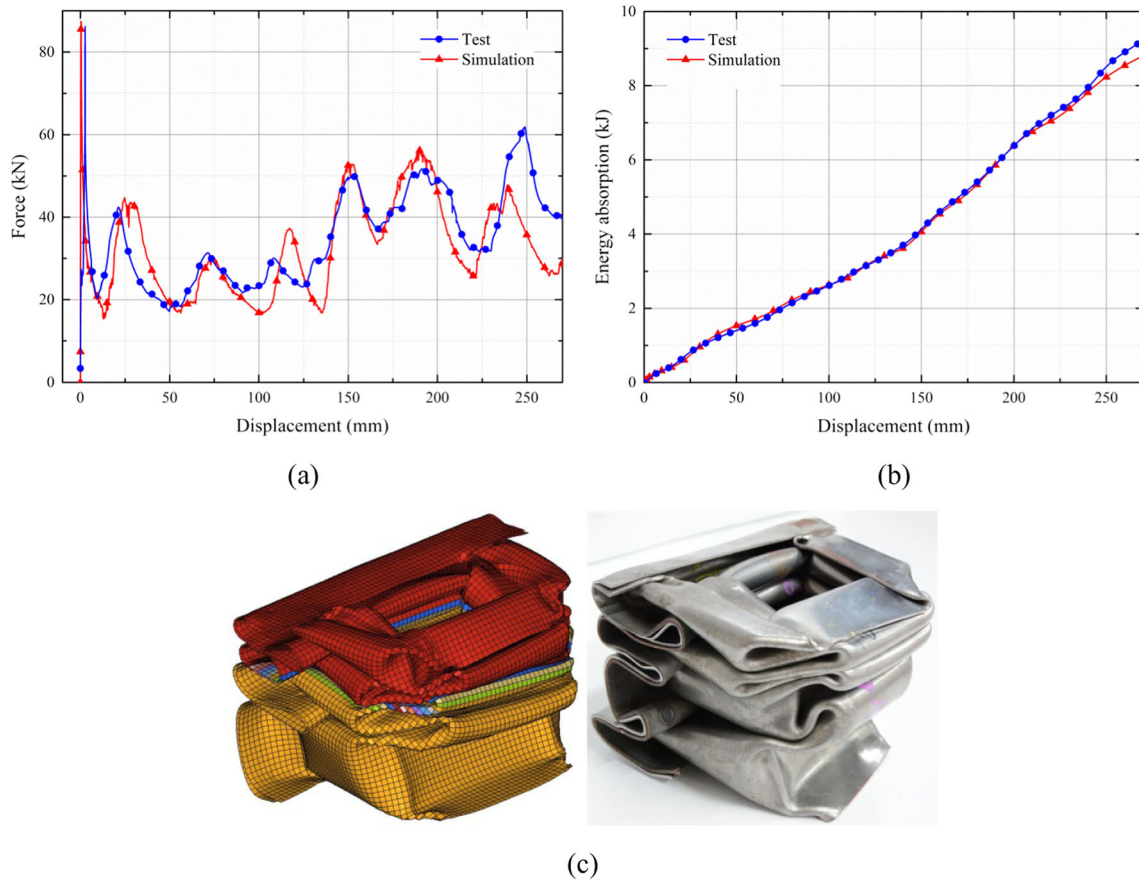


Fig. 9 Comparison between the quasi-static FE simulation and corresponding experimental test: **a** impact force versus displacement curves, **b** energy versus displacement curves, **c** deformation modes under quasi-static axial crushing

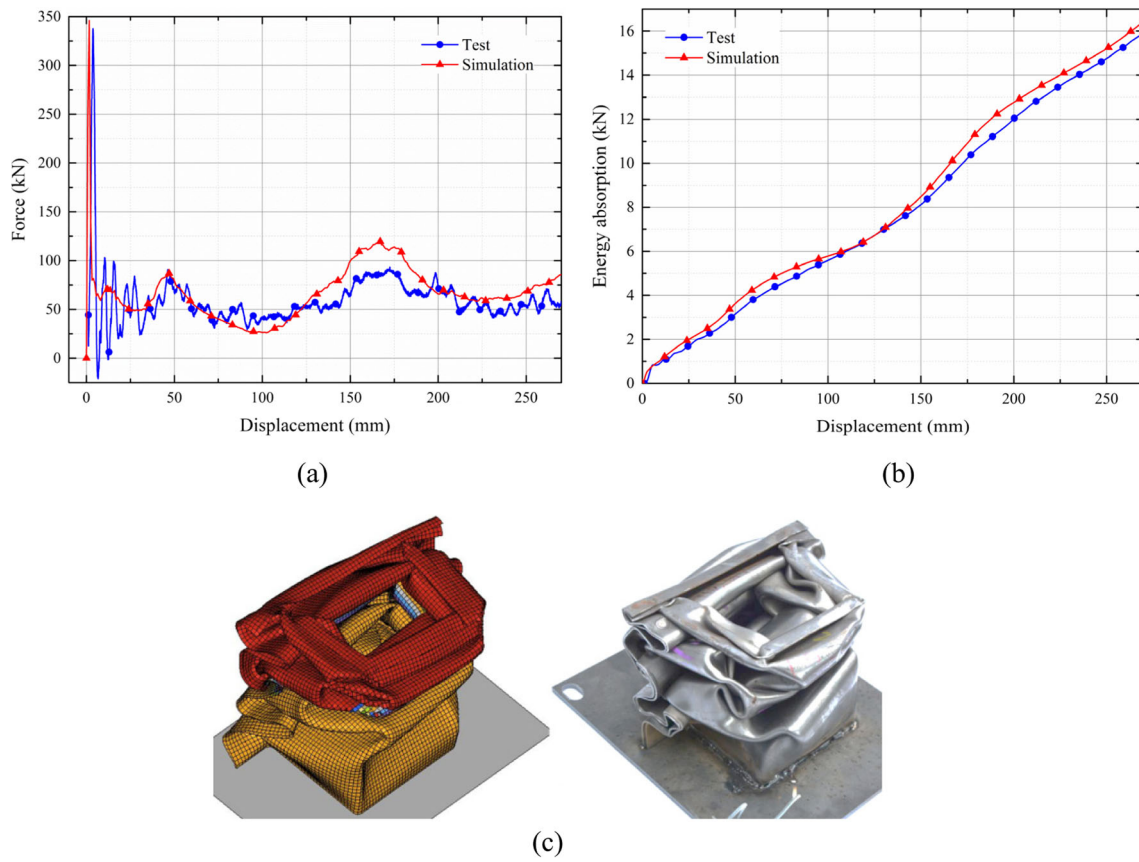


Fig. 10 Comparison between the dynamic FE simulation and corresponding experimental test: **a** impact force versus displacement curves, **b** energy versus displacement curves, **c** deformation models under drop-hammer impact tests.

mathematically as

$$\begin{cases} \min & \left\{ -\sum_{k=1}^q \lambda_k EA_k(t_1, t_2, l_1, w, h), \sum_{k=1}^q \lambda_k M_k(t_1, t_2, l_1, w, h) \right\} \\ \text{s.t.} & F_{\max,k}(t_1, t_2, l_1, w, h) \leq F_{\max,k}^0 \\ & \sum_{k=1}^q \lambda_k = 1 \quad \lambda_k \geq 0 \\ & 1 \leq t_1 \leq t_2 \leq 2 \quad 50 \leq l_1 \leq 250 \quad 80 \leq w \leq 280 \quad 60 \leq h \leq 100 \end{cases} \quad (13)$$

where $F_{\max,k}^0$ is the limit to the peak force; the thicknesses of thin and thick zones (t_1, t_2), the location of TTZ (l_1) and sectional dimensions (w, h) are chosen as the design variables, seen in Fig. 3b.

When the number of loading case, q in Eq. (13), is set as 1, the optimization problem would downgrade to a SLC problem, which represents either the quasi-static loading case or the dynamic loading case herein. $F_{\max,k}^0$ for the quasi-static and the dynamic loading cases were set as 90 kN and 320 kN herein, respectively. When load case number q is set as 2, λ_1 and λ_2 represent the weight factors for the quasi-static loading case and the dynamic loading case, respectively.

To take into account the effects of uncertainties of design variables and obtain the reliable optimal design under MLC, the MOMCRBDO can be formulated as

$$\begin{cases} \min & \left\{ -\sum_{k=1}^q \lambda_k EA_k(t_1, t_2, l_1, w, h), \sum_{k=1}^q \lambda_k M_k(t_1, t_2, l_1, w, h) \right\} \\ \text{s.t.} & P[F_{\max,k}(t_1, t_2, l_1, w, h) \leq F_{\max,k}^0] \geq R_k \\ & \sum_{k=1}^q \lambda_k = 1 \quad \lambda_k \geq 0 \\ & 1 \leq t_1 \leq t_2 \leq 2 \quad 50 \leq l_1 \leq 250 \quad 80 \leq w \leq 280 \quad 60 \leq h \leq 100 \end{cases} \quad (14)$$

where the design feasibility is formulated as the probability ($P[\cdot]$) of constraint satisfaction $F_{\max,k}(t_1, t_2, l_1, w, h) \leq F_{\max,k}^0$ bigger than or equal to a desired probability R_k , which was set as different levels of 90%, 95%, 99% in this study.

To solve the problems defined in Eq. (13) and Eq. (14), the multi-objective optimization procedure was employed based on the RBF metamodels, NSGA-II algorithm with MCS. The detailed parameters of NSGA-II employed herein were summarized in Table 3. It is assumed that all the design variables are normally disturbed with a coefficient of variation of 0.05. For the probabilistic constraints defined in Eq. (14), MCS were performed to estimate the reliability by employing metamodels

Table 2 Parametrical analysis of the TRBHSS

Case	t_1	t_2	l_1	w	h
Case 1	1.2	1.6	180	105	65 (↓)
	1.2	1.6	180	85 (↓)	85
	1.2	1.6	160 (↓)	105	85
	1.2	1.4 (↓)	180	105	85
	1.0 (↓)	1.6	180	105	85
Case 2	1.2	1.6	180	105	75 (↓)
	1.2	1.6	180	95 (↓)	85
	1.2	1.6	170 (↓)	105	85
	1.2	1.5 (↓)	180	105	85
	1.1 (↓)	1.6	180	105	85
Case 0	1.2	1.6	180	105	85
Case 3	1.3 (↑)	1.6	180	105	85
	1.2	1.7 (↑)	180	105	85
	1.2	1.6	190 (↑)	105	85
	1.2	1.6	180	115 (↑)	85
	1.2	1.6	180	105	95 (↑)
Case 4	1.4 (↑)	1.6	180	105	85
	1.2	1.8 (↑)	180	105	85
	1.2	1.6	200 (↑)	105	85
	1.2	1.6	180	125 (↑)	85
	1.2	1.6	180	105	105 (↑)

instead of FEA runs, where the OLHS was employed to generate 100 sample points and then their responses were extracted from FEA. Based on the simulation results, the RBFs of EA , M and F_{max} under different loading cases can be easily constructed. To analyze the influence of the free shape parameter c on the accuracy of RBFs, $c=0, 0.25, 0.5, 0.75$ and 1 were adopted to construct the metamodels for quasi-static and dynamic loading cases, respectively. 18 new validation points were generated by OLHS and used to evaluate the accuracy of the RBF models. The results of R^2 , $RAAE$ and $RMAE$ were listed in Tables 4 and

5. Although the free shape parameter c has certain effect on the RBF performance, it is hard to say which one is the most suitable for all the cases. In general, regardless of c value, these metamodels are considered sufficiently accurate to be employed in the crashworthiness design. Furthermore, some researchers (Gu et al. 2013b; Xu 2015; Xu et al. 2013) found that $c=0.5$ is suitable for most crashworthiness problems, thus $c=0.5$ is adopted herein.

4.2 Result of MORBDO under different SLC

Figure 13 presents the Pareto fronts for the deterministic and reliable designs with different reliability levels under the quasi-static loading case and dynamic loading case, respectively. It can be clearly observed that these two objective EA and M conflict with each other for all the cases, indicating that any increase in EA always leads to an undesirable increase in M , and vice versa. Although the shapes of the Pareto fronts under different reliability levels look similar, their ranges change fairly evidently. That is to say, the uncertainties of design variables have an important influence on the crashworthiness of the TRBHS. More specifically, the Pareto front of the reliable design was further away from the deterministic design when the reliability level increases.

Furthermore, it can be noted that the Pareto fronts can be divided into an insensitive region in the upper-left and a sensitive region in the lower-right. The insensitive region possesses a smaller mass, which would possibly result in a lower peak force and push the design far away from the constraint boundary. Thus, this region has a higher reliability, where the Pareto fronts of deterministic design and reliable design almost coincide. On the contrary, the sensitive region had a lower reliability and the Pareto front of reliable design was pushed away from the deterministic counterpart.

Although the Pareto fronts provide the designer with a great number of solutions over the Pareto space,

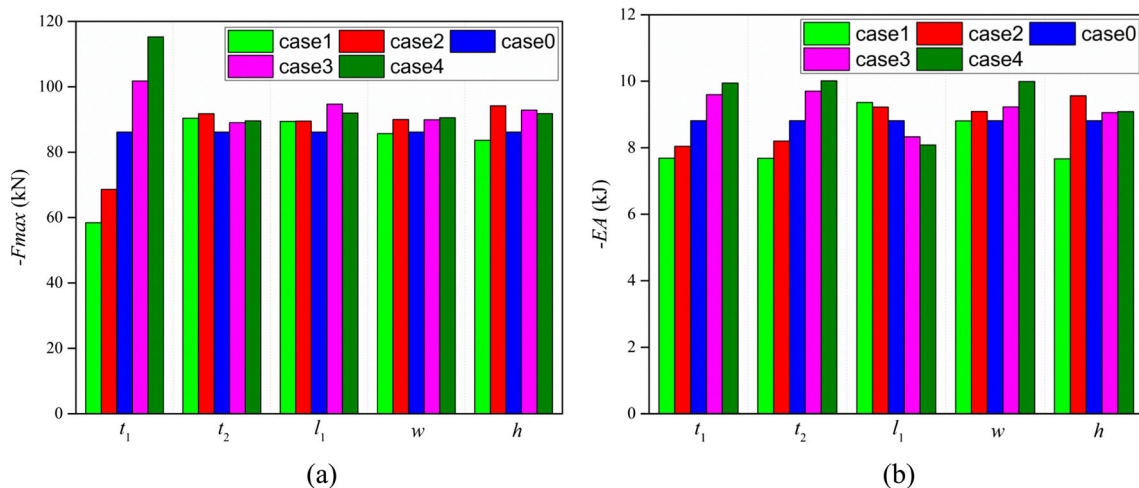


Fig. 11 Variation of **a** F_{max} and **b** EA for different design parameters under quasi-static crushing

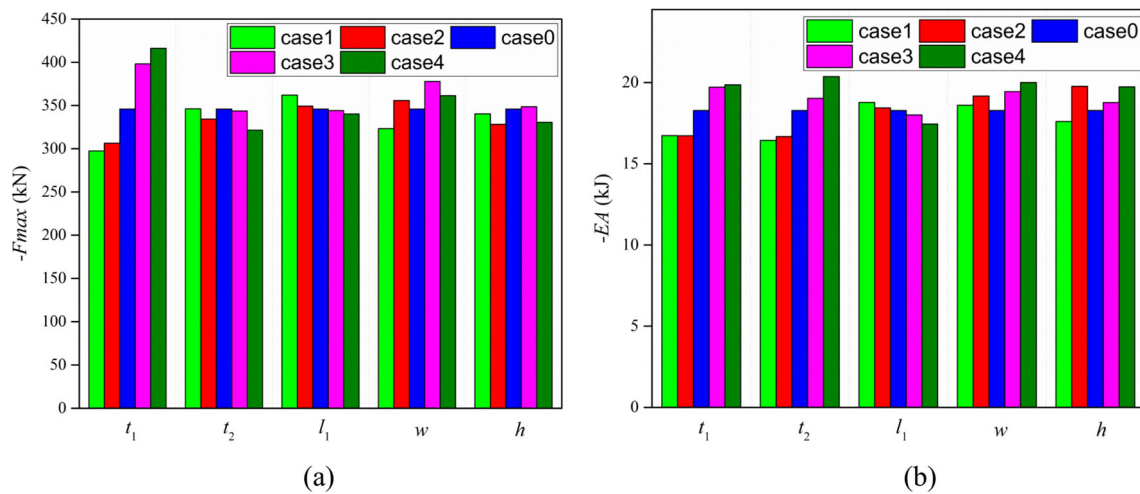


Fig. 12 Variation of **a** F_{max} and **b** EA for different structural parameters under dynamic crushing

Table 3 Details of the NSGA-II parameters used in this study

NSGA-II parameter name	Value
Population size	100
Generation	100
Probability of crossover	0.9
Distribution index for crossover	10
Distribution index for mutation	20

decision must be made for the most satisfactory solution from the Pareto-sets. The minimum distance selection method (TMDSM) (Sun et al. 2010) was employed herein to obtain the most satisfactory solution (namely a Knee point) for different loading cases. A brief overview of the TMDSM was presented in the Appendix. The reliable optima for $R=90\%$, 95% , 99% along with the deterministic optimum and baseline design were summarized in Tables 6 and 7. And MCS with 100, 500, 800 and 1000 samples were conducted, respectively, at each optimum to obtain the corresponding reliabilities. It turned out that 1000 MCSs was adequate herein. The reliabilities of the constraints were also presented in

Tables 7 and 8. The relative error of the deterministic optimal design was summarized in Table 8. It can be seen easily that the maximum error was less than 6.6%, which indicates that the metamodel-based optimization was reasonably accurate. From Tables 6 and 7, it can be seen that both the deterministic design and reliable design can improve the crashworthiness of the TRBHS. However, the reliability of the deterministic optimum was very low. The crashworthiness of TRBHS gradually decreased when the reliability requirement increases from 90% to 99%. Therefore, a compromise should be made between the desired reliability level and the objective performances in practical applications.

4.3 Result of MOMCRBDO

Because the impacting velocity was really unpredictable in car accidents, Therefore, it is essential and practical to consider the uncertainty of the collision velocity in designing the energy-absorbing structures. To take into account the effects of multiple load cases, the weighting factor approach, as formulated in Eqs. (13) and (14), was adopted. To investigate the effect of weighting

Table 4 Accuracy evaluation for different free shape parameter c under quasi-static loading case

c	EA			M			F_{max}		
	R^2	$RAAE$	$RMAE$	R^2	$RAAE$	$RMAE$	R^2	$RAAE$	$RMAE$
0	0.9832	0.1361	2.081	0.9996	0.0207	1.775	0.9858	0.1393	1.789
0.25	0.9854	0.1326	1.889	0.9997	0.0193	1.987	0.9887	0.1305	1.632
0.5	0.9873	0.1273	1.698	0.9997	0.0173	1.144	0.9877	0.1355	1.375
0.75	0.9886	0.1222	1.677	0.9993	0.0287	1.905	0.9906	0.1350	1.311
1	0.9865	0.1175	1.706	0.9998	0.0134	1.742	0.9855	0.1360	1.457

Table 5 Accuracy evaluation for different free shape parameter c under dynamic loading case

c	EA			M			F_{max}		
	R^2	$RAAE$	$RMAE$	R^2	$RAAE$	$RMAE$	R^2	$RAAE$	$RMAE$
0	0.9646	0.2037	2.1421	0.9974	0.3590	2.230	0.8938	0.3690	2.012
0.25	0.9644	0.1999	2.2365	0.9633	0.2989	2.583	0.9072	0.3427	2.063
0.5	0.9648	0.1972	2.256	0.9946	0.2281	1.755	0.9263	0.3219	2.117
0.75	0.9647	0.1962	2.257	0.9487	0.1731	2.851	0.9227	0.3057	2.168
1	0.9675	0.1899	2.206	0.9697	0.1317	2.884	0.9276	0.2917	2.218

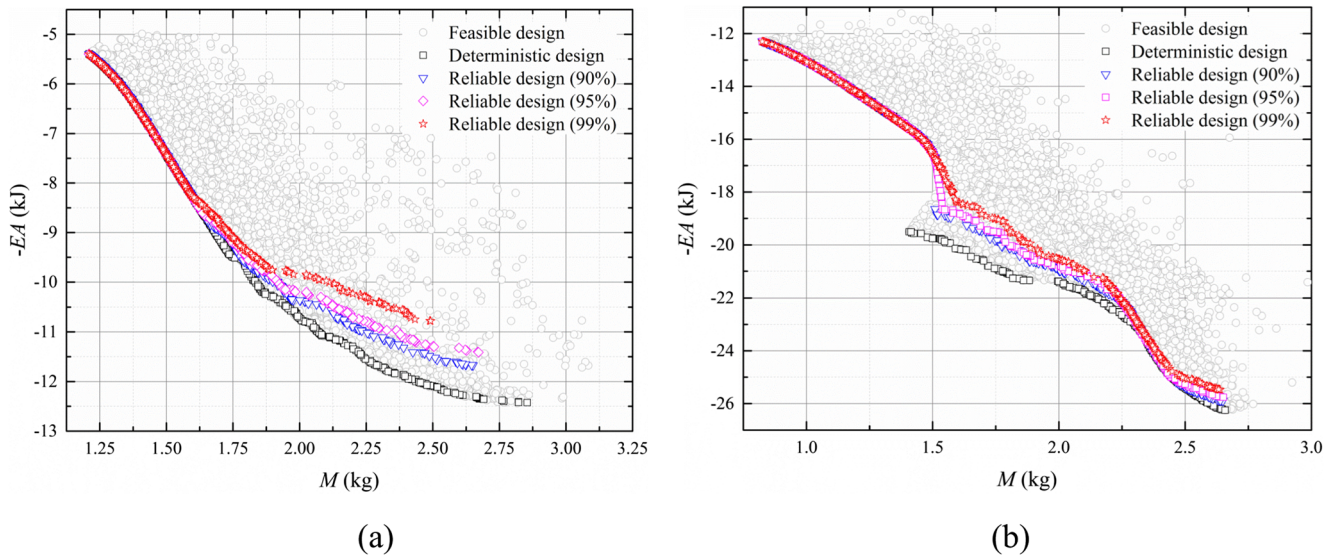


Fig. 13 Pareto fronts for **a** quasi-static loading case; and **b** dynamic loading case

factors on the optimum, three design cases were considered here to emphasize static and dynamic crash differently, as follows:

$$\begin{cases} \text{Case 1: } \lambda_1 = 0.25, \lambda_2 = 0.75 \\ \text{Case 2: } \lambda_1 = 0.5, \lambda_2 = 0.5 \\ \text{Case 3: } \lambda_1 = 0.75, \lambda_2 = 0.25 \end{cases} \quad (15)$$

To compare the deterministic design under SLC and MLC, the corresponding Pareto fronts were plotted in Fig. 14a together. Obviously, the selection of weight

factors for different loading cases had considerable effect on the optimal solution. Taking Case 1 (Fig. 14a) as an example, the Pareto front located fairly closely to the optimal solution generated from the dynamic loading case, while the Pareto fronts generated by the other cases were far away. This was because a heavier weighting factor was placed to the dynamic loading case (i.e., $\lambda_2=0.75$). Similarly, Case 3 assigned a heavier weight to the quasi-static loading case, thus its Pareto front was close to the quasi-static loading solution, as shown in Fig. 14a. The trend of Case 2 was not obvious

Table 6 MCSs at deterministic and reliable optimal design under quasi-static loading case

Response	Baseline	Deterministic	90% Reliable	95% Reliable	99% Reliable
EA	8.8120	10.199	9.5471	9.5594	9.0928
M	2.2480	1.8610	1.7840	1.8084	1.7473
F_{max}	87.143	89.523	79.179	77.416	73.000
Feasibility	/	48.42%	90.87%	94.71%	99.14%

Table 7 MCSs at deterministic and reliable optimal design under dynamic loading case

Response	Baseline	Deterministic	90% Reliable	95% Reliable	99% Reliable
EA	15.933	19.918	18.851	18.667	18.380
M	2.2480	1.5590	1.5173	1.5390	1.5944
F_{max}	336.17	319.46	300.73	296.05	287.55
Feasibility	/	52.47%	90.24%	95.00%	99.15%

Table 8 Error analysis of the deterministic optimal design

Description		EA	M	F_{max}
Quasi-static loading case	Optimal	10.199	1.8610	89.523
	FE model	9.6800	1.8560	94.653
	error %	5.08%	0.27%	-5.73%
Dynamic loading case	Optimal	19.918	1.5590	319.46
	FE model	18.519	1.6410	327.18
	Error (%)	-5.06%	-6.60%	-3.93%

because it emphasized all the loading cases equally. The difference of these Pareto fronts indicates that the selection of weighting factors for different loading cases was critical in the MOMCRBDO solution. Therefore, weighting factors for different loading case should be determined based on the occurrence frequency or statistical data in real life.

Fig. 15 compared the Pareto solutions of MLC for different weighting factors under quasi-static and dynamic loading. From which, it is easily found that the

optimal solution under quasi-static loading case may not be an optimum in dynamic loading case, and *vice versa*. The specific solution to the quasi-static loading case was able to simultaneously reduce the M and enhance the EA compared to the dynamic loading case. That is to say, the optimal designs for SLC only favored a specific loading case. When the designs were subjected to other loading case, the crashworthiness would deteriorate to a certain extent. It is interesting to note that the Pareto fronts for MLC were all located not far away from the corresponding Pareto fronts for SLC in the design space as shown in Fig. 15. That is to say, although the optimal designs under MLC are not able to obtain the optimal solutions for a specific single case, they can obtain a range of compromise solutions for the MLC.

To obtain the reliable optimal design for MLC, the MOMCRBDO were performed at different reliability levels (i.e., $R=90\%$, 95% , 99%) and the optimal results were plotted in Fig. 14c-d. It can be easily seen that the range of Pareto front with MOMCRBDO was

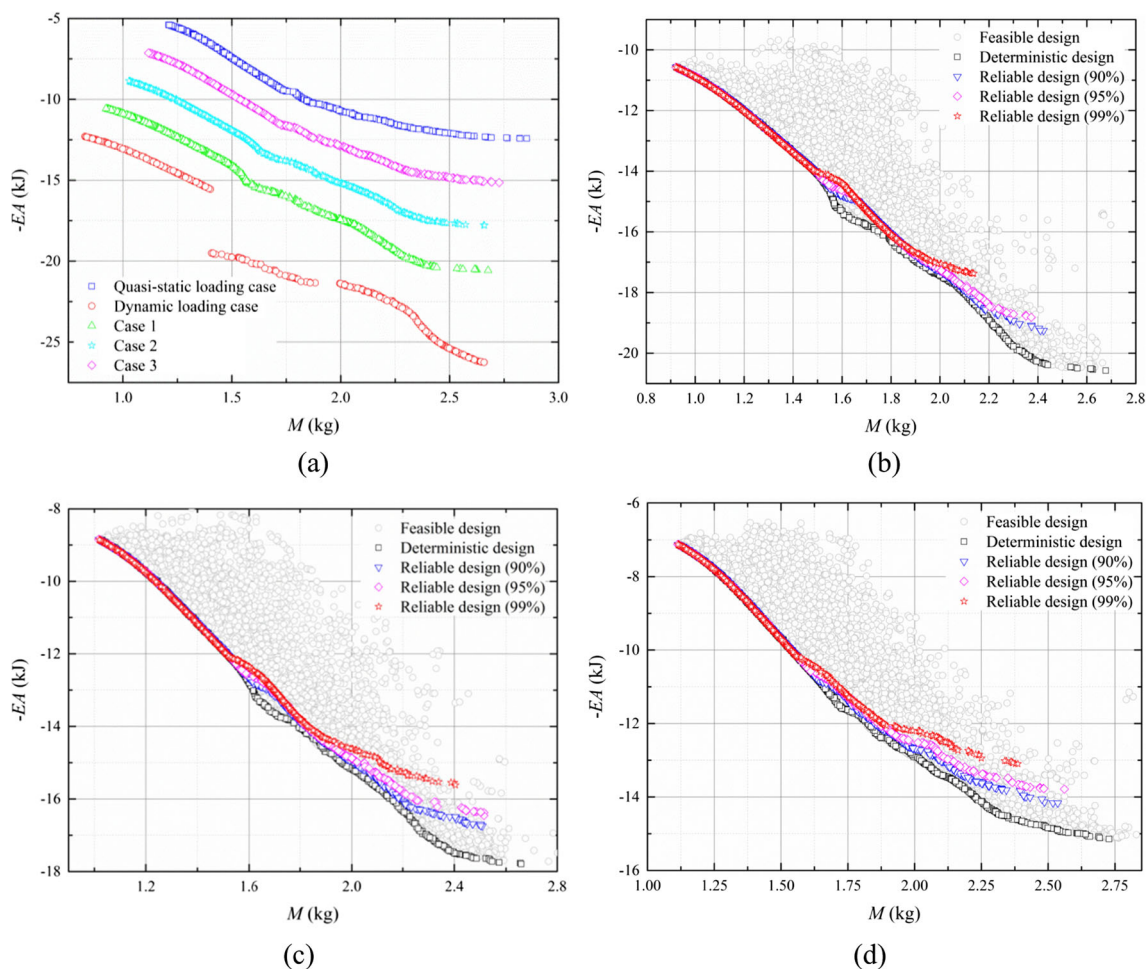


Fig. 14 Pareto fronts for **a** deterministic design **b** reliable design of Case 1 **c** reliable design of Case 2 and **d** reliable design of Case 3

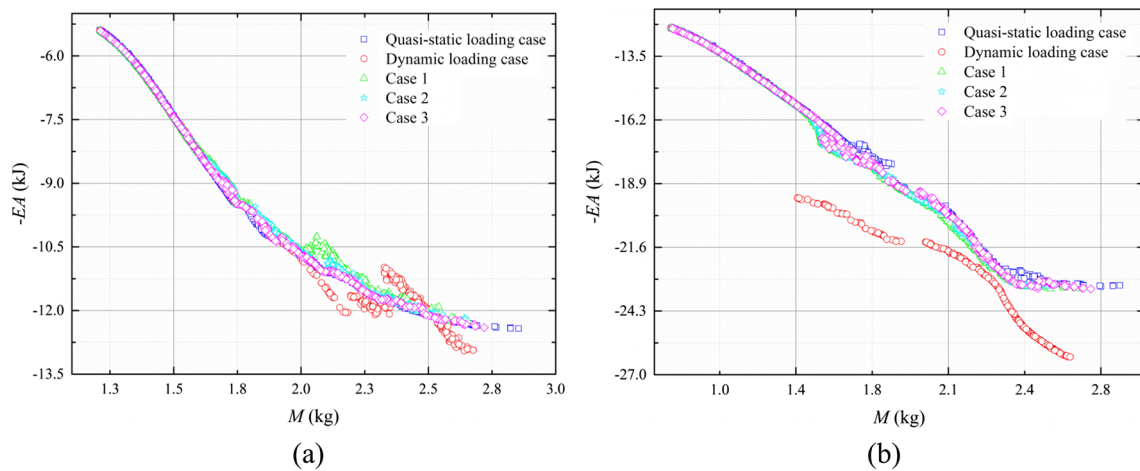


Fig. 15 Pareto Solutions of MLC for different weighting factors: a quasi-static loading case b dynamic loading case

Table 9 MCSs at deterministic and reliable optimal design (Case 1)

Response	Baseline	Deterministic	90% Reliable	95% Reliable	99% Reliable
EA	14.152	15.584	14.711	14.499	14.220
M	2.2480	1.6381	1.5769	1.5556	1.4917
$F_{max,1}/F_{max,2}$	87.248/336.17	89.975/279.83	81.214/272.33	79.016/270.74	74.951/271.27
Feasibility	/	50.43%/94%	90.4%/99%	95.34%/100%	99.04%/99.98%

significantly less than the MODDO for MLC, and the Pareto fronts of the reliable design moved gradually toward right as the reliability requirement increases. In other words, the EA needs to be decreased to accommodate the uncertainty of design variables in MOMCRBDO. This phenomenon is consistent with the results of MORBDO for SLC.

To obtain the most satisfactory solution from the Pareto-fronts, the TMDSM was employed and the optimum results were listed in Tables 9, 10 and 11, respectively. The MCS with 1000 samples were also performed at each optimum to obtain the corresponding reliability. Compared with the baseline design, it can be seen that the MOMCDDO solution can improve the crashworthiness of the TRBHS, but is worse than the deterministic optimal solutions. In addition, the reliability of the reliable optimal solution was higher. This

means that although the objective performances were sacrificed, the reliability of design increased significantly through MOMCRBDO.

5 Conclusions

Vehicular crashworthiness design without considering the random nature of design variables and unpredictability of collision would reduce the reliability of structures. Based on the reliability-based multi-objective design strategy, the tailor rolling blank hat-shaped (TRBHS) structure was optimized in this study. To systematically investigate the crashworthiness of the TRBHS structure, the FE modeling was developed and the corresponding FE analysis was conducted by employing the explicit nonlinear FE code LS-DYNA. Then the quasi-static

Table 10 MCSs at deterministic and reliable optimal design (Case 2)

Response	Baseline	Deterministic	90% Reliable	95% Reliable	99% Reliable
EA	12.373	13.601	13.669	13.920	13.328
M	2.2480	1.6881	1.7690	1.8093	1.7368
$F_{max,1}/F_{max,2}$	87.248/336.17	89.999/276.85	79.397/280.92	76.781/271.26	71.945/270.33
Feasibility	/	50%/96%	90.24%/94.34%	95.16%/99.88%	99.06%/99.93%

Table 11 MCSs at deterministic and reliable optimal design (Case 3)

Response	Baseline	Deterministic	90% Reliable	95% Reliable	99% Reliable
EA	10.592	12.263	11.625	11.506	11.145
M	2.2480	1.8527	1.7821	1.7771	1.7343
$F_{max,1}/F_{max,2}$	87.248/336.17	89.766/300.29	79.524/287.68	76.928/275.72	72.119/273.69
Feasibility	/	48.62%/87.37%	89.78%/98.07%	95.10%/99.83%	99.31%/99.88%

axial crushing and drop-hammer impact tests were performed to validate the FE models. The uncertainties in key geometric dimensions and weighting factors for different loading cases were considered, and NSGA-II and MCS were integrated to seek the Pareto fronts for the multi-objective and multi-case reliability-based design optimization (MOMCRBDO) problems. To provide the decision-maker with insightful information, the MODDO and MORBDO were conducted to maximize the energy absorption and minimize the mass simultaneously under single and multiple loading cases respectively. From the Pareto fronts, it can be seen that the proposed method is not only capable of improving the reliability of Pareto solutions, but also generates more competent solution to the crashworthiness for MLC. Finally, the selected optimums from these Pareto fronts demonstrate that the objective performances could be sacrificed somewhat to satisfy the reliability constraints compared with MODDO, indicating that compromise should be made between the desired reliability level and objective performances in crashworthiness design.

Nevertheless, there exist some limitations in this work. Firstly, this study considered only the uncertainties in geometrical dimensions as well as unpredictability of collision velocity. Despite their critical importance to optimization of TRB structure, other uncertainties, such as collision direction, can affect the reliability of the optimal solutions to some extent, which should be taken into account. Secondly, the weighting factor technique was adopted to combine different loading cases. It turned out that the weighting factors have significant influence on the Pareto’s location, range and shape. For this reason, the weighting factors for different load cases should follow the statistical data and/or occurrence frequency under multiple impact velocity in real life. Thirdly, the MOMCRBDO presented in this paper used the RBF metamodels to approximate the responses. However, for multi-variable problems, constructing a fine RBF metamodel requires substantial number of FE analyses, whose computational cost may become prohibitive in more complex problems.

Acknowledgments This work is supported by National Natural Science Foundation of China (51575172, 61232014). Dr Guangyong

Sun is a recipient of Australian Research Council (ARC) Discovery Early Career Researcher Award (DECRA) in the University of Sydney.

Appendix: brief of the minimum distance selection method (TMDSM)

In this study, TMDSM is employed to obtain a most satisfactory solution from the Pareto-sets. Brief description of the TMDSM is provided below.

The TMDSM can be mathematically formulated as (Sun et al. 2010):

$$\min D = \sqrt[N]{\sum_{\tau=1}^n (f_{c\tau} - \min(f_{\tau}(\mathbf{x})))^N} \tag{A1}$$

where $f_{c\tau}$ is the τ th objective value in the c th Pareto set and n is the number of the objective functions, $N=2, 4, 6, \dots$, D is the least distance from the “Knee point” to a “utopia point” (see Fig. 16), which is composed of the optimum value of each objective and normally not attainable in real life problems with conflicting objectives.

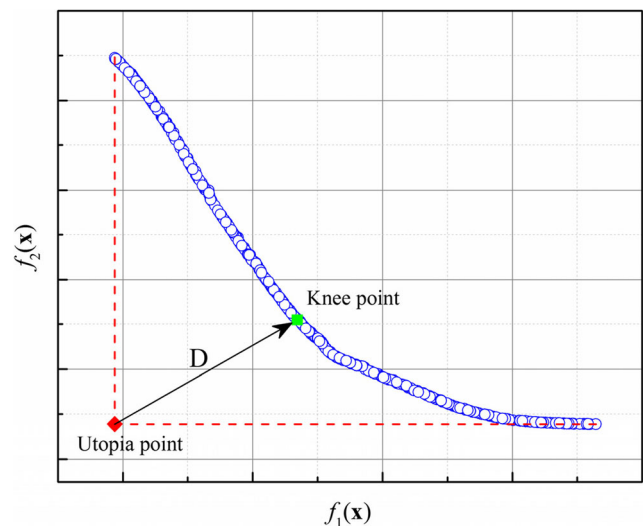


Fig. 16 The knee point on the Pareto front having the least distance from the utopia point

References

- Abdessalem AB, El-Hami A (2015) A probabilistic approach for optimising hydroformed structures using local surrogate models to control failures. *Int J Mech Sci* 96:143–162
- Acar E, Guler M, Gerceker B, Cerit M, Bayram B (2011) Multi-objective crashworthiness optimization of tapered thin-walled tubes with axisymmetric indentations. *Thin-Walled Struct* 49:94–105
- Chen Z, Qiu H, Gao L, Li P (2013) An optimal shifting vector approach for efficient probabilistic design. *Struct Multidiscip Optim* 47:905–920
- Cheng G, Xu L, Jiang L (2006) A sequential approximate programming strategy for reliability-based structural optimization. *Comput Struct* 84:1353–1367
- Choi SK, Grandhi R, Canfield RA (2006) Reliability-based structural design. Springer Science & Business Media
- Chuang C, Yang R, Li G, Mallela K, Pothuraju P (2008) Multidisciplinary design optimization on vehicle tailor rolled blank design. *Struct Multidiscip Optim* 35:551–560
- Deb K, Pratap A, Agarwal S, Meyarivan T (2002) A fast and elitist multiobjective genetic algorithm: NSGA-II. *IEEE Trans on Evolutionary Computation* 6:182–197
- Du X, Chen W (2004) Sequential optimization and reliability assessment method for efficient probabilistic design. *J Mech Des* 126:225–233
- Duan L, Sun G, Cui J, Chen T, Cheng A, Li G (2016) Crashworthiness design of vehicle structure with tailor rolled blank. *Struct Multidiscip Optim* 53:321–338
- Duddeck F, Wehrle E (2015) Recent advances on surrogate modeling for robustness assessment of structures with respect to crashworthiness requirements. 10th European LS-DYNA Conference 2015, Wurzburg, Germany
- Fang H, Rais-Rohani M, Liu Z, Horstemeyer MF (2005) A comparative study of metamodeling methods for multiobjective crashworthiness optimization. *Comput Struct* 83:2121–2136
- Fang J, Gao Y, Sun G, Li Q (2013) Multiobjective reliability-based optimization for design of a vehicle door. *Finite Elem Anal Des* 67:13–21.
- Fang J, Gao Y, Sun G, Zhang Y, Li Q (2014) Crashworthiness design of foam-filled bitubal structures with uncertainty. *Int J Non Linear Mech* 67:120–132
- Fang J, Gao Y, Sun G, Qiu N, Li Q (2015a) On design of multi-cell tubes under axial and oblique impact loads. *Thin-Walled Struct* 95:115–126
- Fang J, Gao Y, Sun G, Xu C, Li Q (2015b) Multiobjective robust design optimization of fatigue life for a truck cab Reliability. *Reliab Eng Syst Saf* 135:1–8
- Fang J, Sun G, Qiu N, Kim NH, Li Q (2016) On design optimization for structural crashworthiness and its state of the art. *Struct and Multidiscip Optim*. doi:10.1007/s00158-016-1579-y
- Gu L, Yang R (2005) On reliability-based optimisation methods for automotive structures International. *Int J Mater Prod Technol* 25:3–26
- Gu X, Sun G, Li G, Huang X, Li Y, Li Q (2013a) Multiobjective optimization design for vehicle occupant restraint system under frontal impact. *Struct Multidiscip Optim* 47:465–477
- Gu X, Sun G, Li G, Mao L, Li Q (2013b) A comparative study on multiobjective reliable and robust optimization for crashworthiness design of vehicle structure. *Struct Multidiscip Optim* 48:669–684
- Hallquist JO (2007) LS-DYNA keyword user's manual. Livermore Software Technology Corporation 971
- Hardy RL (1971) Multiquadric equations of topography and other irregular surfaces. *J Geophys Res-Atmos* 76:1905–1915
- Hirt G, Abratis C, Ames J, Meyer A (2005) Manufacturing of sheet metal parts from tailor rolled blanks. *J Technol Plasticity* 30:1–12
- Jansson T, Nilsson L, Moshfegh R (2008) Reliability analysis of a sheet metal forming process using Monte Carlo analysis and metamodels. *J Mater Process Technol* 202:255–268
- Jiang C, Shan Z, Zhuang B, Zhang M, Xu Y (2012) Hot stamping die design for vehicle door beams using ultra-high strength steel International. *Int J Precis Eng Manuf* 13:1101–1106
- Jin R, Chen W, Simpson TW (2001) Comparative studies of metamodeling techniques under multiple modelling criteria. *Struct Multidiscip Optim* 23:1–13
- Kim HJ, McMillan C, Keoleian GA, Skerlos SJ (2010) Greenhouse Gas emissions payback for lightweighted vehicles using aluminum and high-strength steel. *J Ind Ecol* 14:929–946
- Kopp R, Wiedner C, Meyer A (2005) Flexibly rolled sheet metal and its use in sheet metal forming. *Adv Mater Res* 6–8:81–92
- Li F, Luo Z, Sun G (2011) Reliability-based multiobjective design optimization under interval uncertainty. *Comput Model Eng Sci* 74:39–64
- Li G, Xu F, Huang X, Sun G (2015) Topology optimization of an automotive tailor-welded blank door. *J Mech Des* 137:055001–055001
- Liao X, Li Q, Yang X, Zhang W, Li W (2008) Multiobjective optimization for crash safety design of vehicles using stepwise regression model. *Struct Multidiscip Optim* 35:561–569
- Melchers RE (1987) Structural reliability. Horwood
- Merklein M, Johannes M, Lechner M, Kuppert A (2014) A review on tailored blanks-production, applications and evaluation. *J Mater Process Technol* 214:151–164
- Pan F, Zhu P, Zhang Y (2010) Metamodel-based lightweight design of B-pillar with TWB structure via support vector regression. *Comput Struct* 88:36–44
- Park JS (1994) Optimal Latin-hypercube designs for computer experiments. *J Stat Plan Inference* 39:95–111
- Qiu N, Gao Y, Fang J, Feng Z, Sun G, Li Q (2015) Crashworthiness analysis and design of multi-cell hexagonal columns under multiple loading cases. *Finite Elem Anal Des* 104:89–101
- Shi Y, Zhu P, Shen L, Lin Z (2007) Lightweight design of automotive front side rails with TWB concept. *Thin-Walled Struct* 45:8–14
- Sun G, Li G, Zhou S, Li H, Hou S, Li Q (2010) Crashworthiness design of vehicle by using multiobjective robust optimization. *Struct Multidiscip Optim* 44:99–110
- Sun G, Li G, Gong Z, He G, Li Q (2011) Radial basis functional model for multi-objective sheet metal forming optimization. *Eng Optim* 43:1351–1366
- Sun G, Li G, Li Q (2012) Variable fidelity design based surrogate and artificial bee colony algorithm for sheet metal forming process finite. *Finite Elem Anal Des* 59:76–90
- Sun G, Xu F, Li G, Li Q (2014) Crashing analysis and multiobjective optimization for thin-walled structures with functionally graded thickness. *Int J Impact Eng* 64:62–74
- Sun G, Fang J, Tian X, Li G, Li Q (2015a) Discrete robust optimization algorithm based on Taguchi method for structural crashworthiness design. *Expert Syst Appl* 42:4482–4492
- Tu J, Choi KK, Park YH (1999) A new study on reliability-based design optimization. *J Mech Des* 121:557–564
- White M, Jones N (1999) Experimental quasi-static axial crushing of top-hat and double-hat thin-walled sections. *Int J Mech Sci* 41:179–208
- Xu F (2015) Enhancing material efficiency of energy absorbers through graded thickness structures. *Thin-Walled Struct* 97:250–265
- Xu F, Sun G, Li G, Li Q (2013) Crashworthiness design of multi-component tailor-welded blank (TWB) structures. *Struct Multidiscip Optim* 48:653–667

- Yang R, Gu L (2004) Experience with approximate reliability-based optimization methods. *Struct Multidiscip Optim* 26: 152–159
- Youn BD, Choi KK (2004) A new response surface methodology for reliability-based design optimization. *Comput Struct* 82:241–256
- Zhang Y, Lai X, Zhu P, Wang W (2006) Lightweight design of automobile component using high strength steel based on dent resistance. *Mater Des* 27:64–68
- Zhang Y, Sun G, Xu X, Li G, Li Q (2014) Multiobjective crashworthiness optimization of hollow and conical tubes for multiple load cases. *Thin-Walled Struct* 82:331–342
- Zhu P, Zhang Y, Chen G (2011) Metamodeling development for reliability-based design optimization of automotive body structure. *Comput Ind* 62:729–741